Commun. Theor. Phys. **76** (2024) 115402 (13pp) https://doi.org/10.1088/1572-9494/ad5d90

Thermal fluctuations, deflection angle, and greybody factor of a high-dimensional Schwarzschild black hole in scalar–tensor–vector gravity

Qian Li, Yu Zhang*, Qi-Quan Li and Qi Sun

Faculty of Science, Kunming University of Science and Technology, Kunming, Yunnan 650500, China

E-mail: zhangyu_128@126.com

Received 31 March 2024, revised 26 May 2024
Accepted for publication 2 July 2024
Published 21 August 2024

Abstract

In this study, we examined the thermal fluctuations, deflection angle, and greybody factor of a high-dimensional Schwarzschild black hole in scalar–tensor–vector gravity (STVG). We calculated some thermodynamic quantities related to the correction of the black hole entropy caused by thermal fluctuations and discussed the effect of the correction parameters on these quantities. By analyzing the changes in the corrected specific heat, we found that thermal fluctuations made the small black hole more stable. It is worth noting that the STVG parameter did not affect the thermodynamic stability of this black hole. Additionally, by utilizing the Gauss–Bonnet theorem, the deflection angle was obtained in the weak field limit, and the effects of the two parameters on the results were visualized. Finally, we calculated the bounds on the greybody factor of a massless scalar field. We observed that as the STVG parameter around the black hole increased, the weak deflection angle became larger, and more scalar particles can reach infinity. However, the spacetime dimension has the opposite effect on the STVG parameter on the weak deflection angle and greybody factor.

Keywords: black hole, thermal fluctuations, deflection angle, greybody factor

1. Introduction

Although Einstein's general relativity is one of the successful and well-established gravitational theories in modern physics, it fails to explain many observational results, such as the present stage of cosmic acceleration [1], rotation curves of galaxies [2], and some cosmological data [3]. Moreover, general relativity has inherent deficiencies in theory, including the presence of spacetime singularities. Therefore, the problems of general relativity motivated us to research alternative gravity theories. One of the modified theories of gravity is the scalar–tensor–vector gravity (STVG) theory proposed by Moffat [4], which is based on the action principle and introduces three scalar fields and a vector field. Moreover, this modified gravity (MOG), i.e. STVG, may offer an alternative to the dark matter issue by introducing changes in the gravity sector. Specifically, the STVG theory was able to explain the rotation curves of galaxies [5] without the need for dark matter and exhibited no deviation in Solar System observational tests. This is because the STVG theory necessitates the variation of the gravitational constant G, a vector field coupling constant ω, and the vector field mass $\tilde{\mu}$ with respect to distance and time. Moffat provided a black hole solution in the STVG theory in another paper [4]. This solution considers the dimensionless constant $\omega = 1$ and neglects the effect of the vector field mass $\tilde{\mu}$. Furthermore, it assumes that G is a constant dependent on a, i.e. $G = G_{\mathrm{N}}(1 + a)$, where G_{N} is Newton's constant. It is very clear that parameter a is used to quantify the strength of the gravitational field and is regarded as a deviation parameter from the standard general relativity theory by the STVG theory. Later, several studies in the literature were dedicated to exploring various black hole solutions in the context of the STVG theory [6–9]. However, Jamali *et al* [10] found that a modified version

* Author to whom any correspondence should be addressed.

of the STVG, known as mMOG, cannot be considered as an alternative to the dark matter problem when new constants are introduced in the kinetic term of the scalar field as its coefficients. In addition, some studies have been conducted to understand the characteristics of different black holes within the framework of the STVG theory [11–14].

Despite the absence of direct observation or experimental support for high-dimensional black holes in comparison with four-dimensional black holes, there has been a notable increase in interest in the physical characteristics of high-dimensional black holes. This has a lot to do with the development of string theory. For example, the Bekenstein–Hawking entropy relation, which is proportional to the area of the event horizon of a black hole [15], was derived in string theory for a five-dimensional black hole [16]. In addition, we have to mention the anti-de Sitter/conformal field theory (AdS/CFT) correspondence or gauge–string duality. This technique relates the classical dynamics of D-dimensional gravity to the quantum physics of the dual conformal field theory in $(D-1)$ dimensions [17]. The theoretical significance of higher-dimensional black hole solutions was extensively elucidated by Emparan and Reall [18]. Tangherlini [19] first proposed solutions of the Schwarzschild and Reissner–Nordström black holes in D-dimensional spacetime. Later, Myers *et al* obtained the Kerr black hole solution in a higher-dimensional spacetime [20]. Recently, Cai *et al* [21] derived a higher-dimensional static spherically symmetric Schwarzschild black hole in the STVG theory, which is a high-dimensional extension of the STVG theory, and studied its quasinormal modes of a massless scalar field and black hole shadow. This black hole solution is a link between Einstein's theory and the STVG theory. Specifically, this black hole degenerates to the Schwarzschild–Tangherlini black hole in Einstein's theory, with a coupling constant a of zero.

Hawking believed that black holes are not completely black objects and can emit radiation known as Hawking radiation [22, 23]. This lays an important foundation for understanding the thermodynamics of black holes. Black holes also adhere to the four laws of black hole mechanics, which bear resemblance to the laws of thermodynamics. As can be seen from the second law of black hole thermodynamics, the black hole entropy is maximum compared with objects of the same volume. However, due to the thermal fluctuations that lead to the concept of the holographic principle [24], the maximum entropy of black holes may be corrected. The correction term in the maximum entropy is generated by the quantum fluctuations in the spacetime geometry rather than the matter field in spacetime. Generally, quantum fluctuations are negligible for large black holes; thus, large black holes are considered to be thermodynamically stable. When the size of a black hole is reduced due to Hawking radiation, the quantum fluctuations in the spacetime geometry increase, and the black hole becomes unstable. However, there are cases where small black holes are thermodynamically stable [25–27]. The presence of a logarithmic correction at the leading order in black hole entropy explains this phenomenon [28]. Upadhyay investigated the effect of thermal fluctuations on a quasitopological black hole and found that the negative correction term leads to a local instability of black hole [29]. The influence of a logarithmic correction on the thermodynamics due to thermal fluctuations for a dilaton black hole in gravity's rainbow was studied in [30]. A number of studies have been devoted to studying the effects of thermal fluctuations on black hole thermodynamics [31–37].

The Hawking radiation detected at infinity of the black hole differs by a redshift factor, called greybody factor, from the authentic radiation detected at the black hole horizon due to the existence of a potential barrier. The greybody factor derived from the transmission amplitude can provide information related to the quantum nature of black holes [38]. Additionally, it can be used to approximate the part of the initial quantum radiation that is reflected back by the potential barrier close to the event horizon [39]. In other words, the waves coming from infinity are partially absorbed by the black hole, and the absorption rate (probability of crossing the barrier) is referred to as the greybody factor. The greybody factor has the same meaning in both cases. When one considers a test field with suitable boundary conditions, such as a scalar field impinging on a black hole, the greybody factor is crucial not only for understanding the classical scattering problem but also for estimating the intensity of the Hawking radiation. There are several methods for calculating the greybody factor, such as the bounds on the greybody factor [40–43], Wenzel–Kramers–Brillouin (WKB) method [44–48], and exact numerical approach [49–51]. In this study, we chose the bounds on the greybody factor because it can provide analytical results for the intermediate frequencies and all angular momenta.

Because of its strong gravitational force, the spacetime around a massive central object is no longer flat. Consequently, when a light ray encounters a compact object in its trajectory toward a distant observer, the observer observes a deflection angle in the light ray. This phenomenon, known as gravitational lensing, occurs when a compact object bends a light ray. Gravitational lensing, which can be classified as strong gravitational lensing, weak gravitational lensing, or microgravitational lensing, is used as a specialized astronomical tool to verify the correctness of the general theory of relativity. Specifically, the strong gravitational lensing is employed to determine the magnification and position of black holes. The weak gravitational lensing can help us measure the masses of different objects or restrict the cosmological parameter. In addition, weak gravitational lensing also has an important effect on the cosmic microwave background aspects [52–54]. At present, the study of the strong or weak gravitational lensing of compact objects, such as wormholes, black holes, and cosmic strings, has gained significant attention [55–74, 75, 76]. Part of the studies in the aforementioned literature is based on Gauss–Bonnet theorem for calculating the deflection angle for the weak gravitational lensing. The Gauss–Bonnet theorem, proposed by Gibbon and Werner [77] in 2008, was used for the first time to derive the deflection angle in the context of optical geometry. Since then, this method has been applied to calculate the weak deflection angle of various black holes [78–88]. We intend to investigate the weak deflection angle in high-dimensional Schwarzschild spacetime within the framework of the STVG theory using the Gauss–Bonnet theorem. This will help us to gain a deeper understanding of the geometry of this black hole. Since the 1970s, the scattering problem caused by plane waves impinging on black holes has been of interest. Similar to Rutherford scattering, a classical formula that involves the deflection angle (i.e. the classical differential scattering cross

section) describes the intensity of scattering by black holes [89]. Therefore, in addition to the use of weak deflection angles in weak gravitational lensing, it is used to approximately estimate the classical differential scattering cross section for small angles.

To gain a more comprehensive understanding of this black hole, we conducted studies from the perspectives of quantum and geometry. At the quantum level, using Hawking radiation as a starting point, we explored issues related to black hole thermodynamics and greybody factor to help us understand the physical properties and behavior of this black hole. In terms of geometry, we focused on the phenomenon of weak deflection angles. This not only deepened our understanding of the geometry of space around black holes but also provided crucial experimental evidence for exploring and verifying modified theories of gravity, thereby helping us reveal more details about the nature of MOG. Through these two aspects of research, we hope that this study will help us describe and predict the behavior of black holes and their impact on the surrounding matter. The remainder of this paper is structured as follows. In section 2, we briefly introduce a high-dimensional Schwarzschild black hole solution in the STVG theory. We then review the physical features of this black hole. In section 3, we study the corrected thermodynamic quantities due to thermal fluctuations. Section 4 presents the calculation of the weak deflection angle using the Gauss–Bonnet theorem. We discuss the bounds on the greybody factor in section 5. Our conclusions are summarized in the last section.

Throughout this paper, a natural system of units ($G_{\rm N}=\hbar=c=1$) is adopted.

2. Fundamental spacetime

In this section, we introduce high-dimensional Schwarzschild spacetime in the STVG theory and review some thermodynamic properties. The general action of the STVG theory in D-dimensional spacetime takes the form [6]

$$S_{\rm L}=S_{\rm GR}+S_{\phi}+S_{\rm S}+S_{\rm M}, \tag{1}$$

where

$$\begin{aligned} S_{\rm GR}&=\frac{1}{16\pi}\int {\rm d}^Dx\sqrt{-g}\frac{1}{G}R,\\ S_{\phi}&=-\frac{1}{4\pi}\int {\rm d}^Dx\sqrt{-g}\left(K-\frac{1}{2}\tilde{\mu}^2\phi^{\mu}\phi_{\mu}\right),\\ S_{\rm S}&=\int {\rm d}^Dx\sqrt{-g}\left[\frac{1}{G^3}\left(\frac{1}{2}g^{\mu\nu}\nabla_{\mu}G\nabla_{\nu}G-V_{\rm G}(G)\right)\right.\\ &\quad\left.+\frac{1}{\tilde{\mu}^2G}\left(\frac{1}{2}g^{\mu\nu}\nabla_{\mu}\tilde{\mu}\nabla_{\nu}\tilde{\mu}-V_{\tilde{\mu}}(\tilde{\mu})\right)\right], \end{aligned} \tag{2}$$

where $S_{\rm GR}$ is the Einstein–Hilbert action, S_{ϕ} stands for the action of a massive vector field ϕ^{μ}, $S_{\rm S}$ denotes the action of the scalar field, $S_{\rm M}$ represents the matter action, and ϕ_{μ} is a massive vector field (Proca type) with mass $\tilde{\mu}$. K, being the kinetic term of the vector field ϕ^{μ}, is usually written as $K=\frac{1}{4}B^{\mu\nu}B_{\mu\nu}$, where the tensor field is defined as $B_{\mu\nu}=\partial_{\mu}\phi_{\nu}-\partial_{\nu}\phi_{\mu}$. $V(G)$ and $V(\tilde{\mu})$ are the two potentials related to the two scalar fields $G(x)$ and $\tilde{\mu}(x)$, respectively.

The black hole metric in the D-dimensional spacetime has the following form:

$${\rm d}s^2=-f(r){\rm d}t^2+\frac{{\rm d}r^2}{f(r)}+r^2{\rm d}\Omega_{D-2}^2, \tag{3}$$

where ${\rm d}\Omega_{D-2}^2$ denotes the metric on a $(D-2)$-dimensional unit sphere, with the line element $f(r)$ as described in [21],

$$f(r)=1-\frac{m}{r^{D-3}}+\frac{Gq^2}{r^{2(D-3)}}, \tag{4}$$

and m and q are defined as

$$\begin{aligned} m&\equiv\frac{16\pi GM}{(D-2)\Omega_{D-2}},\\ q&\equiv\frac{8\pi\sqrt{aG_{\rm N}}M}{\sqrt{2(D-2)(D-3)}\,\Omega_{D-2}}, \end{aligned} \tag{5}$$

where M is the black hole mass. Moreover, Ω_{D-2} denoting the volume of unit $(D-2)$-dimensional sphere has the form,

$$\Omega_{D-2}=\frac{2\pi^{\frac{D-1}{2}}}{\Gamma\left(\frac{D-1}{2}\right)}. \tag{6}$$

When the dimensionless parameter $a=0$, we can get a Schwarzschild–Tangherlini black hole in Einstein's gravity. Moffat gave a Schwarzschild black hole in the STVG theory for the case $D=4$ [6]. Mureika *et al* [90] pointed out that the parameter q of the Schwarzschild black hole in the STVG theory relies only on the mass M and dimensionless parameter a. Thus, q is called the gravitational charge rather than the charge. Moreover, one can find that there is a similarity between a high-dimensional Schwarzschild black hole in the STVG theory and a high-dimensional Reissner–Nordström black hole in Einstein gravity from the metric [26]. The high-dimensional Schwarzschild STVG black hole possesses up to two horizons,

$$r_{\pm}=\left(\frac{m}{2}\pm\frac{\sqrt{m^2-4Gq^2}}{2}\right)^{\frac{1}{D-3}}, \tag{7}$$

where r_- and r_+ represent the Cauchy horizon and the event horizon, respectively.

The black hole mass in terms of r_+ has the form,

$$M=\frac{r_+^{D-3}(A-\sqrt{A^2-4GB^2})}{2GB^2}, \tag{8}$$

where the coefficients A and B are expressed as

$$\begin{aligned} A&\equiv\frac{16\pi G}{(D-2)\Omega_{D-2}},\\ B&\equiv\frac{8\pi\sqrt{aG_{\rm N}}}{\sqrt{2(D-2)(D-3)}\,\Omega_{D-2}}. \end{aligned} \tag{9}$$

The Hawking temperature is given by

$$T_{\rm H} = \frac{1}{4\pi}\frac{{\rm d}f(r)}{{\rm d}r}|_{r=r_+} = \frac{(D-3)(A\sqrt{A^2-4GB^2}-A^2+4GB^2)}{8\pi GB^2 r_+}. \quad (10)$$

In addition, the Bekenstein–Hawking entropy of this high-dimensional black hole S_0 is given by

$$S_0 = \frac{\Omega_{D-2} r_+^{D-2}}{4}. \quad (11)$$

3. Thermal fluctuations

In this section, we investigate the influence of thermal fluctuations on the thermodynamic potential of a high-dimensional Schwarzschild STVG black hole. First, we introduce thermal fluctuations and then calculate some important modified thermodynamic quantities. We cannot neglect the influence of thermal fluctuations on black hole thermodynamics when the radius of the black hole decreases and the temperature of the black hole is large. Thermal fluctuations are regarded as perturbations around the state of equilibrium if they are small enough.

To study the impact of thermal fluctuations on the entropy of a high-dimensional Schwarzschild STVG black hole, we briefly derived the expression of the corrected entropy (see [91] for more details). The partition function employed to derive the corrected entropy is defined as

$$Z(\beta) = \int_0^\infty {\rm d}E\rho(E){\rm e}^{-\beta E}, \quad (12)$$

where $\beta = \frac{1}{T_{\rm H}}$ as Boltzmann constant $k = 1$. The density of states $\rho(E)$ can be calculated by the inverse Laplace transform with the expression,

$$\rho(E) = \frac{1}{2\pi{\rm i}}\int_{\beta_0-{\rm i}\infty}^{\beta_0+{\rm i}\infty}{\rm d}\beta Z(\beta)\exp(\beta E) = \frac{1}{2\pi{\rm i}}\int_{\beta_0-{\rm i}\infty}^{\beta_0+{\rm i}\infty}{\rm d}\beta\exp(S(\beta)), \quad (13)$$

where $S(\beta) = \ln Z(\beta) + \beta E$ is referred to as the modified entropy of the black hole, which depends on the Hawking temperature. Using the Taylor expansion around the extremum β_0 with the aid of the steepest descent method, the corrected entropy is described as

$$S(\beta) = S_0 + \frac{1}{2}(\beta-\beta_0)^2\frac{\partial^2 S(\beta)}{\partial\beta^2}\Big|_{\beta=\beta_0} + {\rm higher-order\ terms}, \quad (14)$$

where S must meet the conditions $\frac{\partial S}{\partial\beta} = 0$ and $\frac{\partial^2 S}{\partial\beta^2} > 0$. Substituting the above equation into equation (13), we obtained

$$\rho(E) = \frac{\exp(S)}{2\pi{\rm i}}\int{\rm d}\beta\exp\left(\frac{1}{2}(\beta-\beta_0)^2\frac{\partial^2 S(\beta)}{\partial\beta^2}\right). \quad (15)$$

By solving for the integral, we obtained the exact expression, which is

$$\rho(E) = \frac{\exp(S)}{\sqrt{2\pi}}\left[\left(\frac{\partial^2 S(\beta)}{\partial\beta^2}\right)\Big|_{\beta=\beta_0}\right]^{-\frac{1}{2}}, \quad (16)$$

and taking the logarithm of this expression, we obtained the expression of the corrected entropy as follows [26, 91]:

$$S = S_0 - \frac{1}{2}\ln(S_0T^2) + \frac{\lambda}{S_0}. \quad (17)$$

Without loss of generality, a general expression for the corrected entropy area relation is written as [92–97]

$$S = S_0 - \alpha\ln(S_0T^2) + \frac{\lambda}{S_0}. \quad (18)$$

Note that to control the effect of logarithmic correction on the corrected entropy, $1/2$ is replaced by the dimensionless parameter α; λ is the second-order correction parameter. The leading-order correction is a logarithmic term caused by thermal fluctuations, and the second-order correction proportional to the inverse to the uncorrected entropy is produced by extending the entropy function around the equilibrium. To better verify the effects of parameters α and λ in subsequent calculations, larger values of parameters α and λ may be chosen.

Using equations (10) and (11), the corrected entropy of this high-dimensional black hole is given as

$$S = \frac{1}{4}r_+^{D-2}\Omega_{D-2} + \frac{4r_+^{2-D}\lambda}{\Omega_{D-2}} - \alpha\ln\left[\frac{(D-3)^2(A^2-4GB^2)(A-\sqrt{A^2-4GB^2})^2 r_+^{D-4}\Omega_{D-2}}{256G^2B^4\pi^2}\right]. \quad (19)$$

We plotted the corrected entropy against the event horizon radius for different parameters in figures 1 and 2. As depicted in figure 1, the presence of the leading-order correction resulted in an increase in entropy for small values of the event horizon radius. However, the corrected entropy gradually decreased and returned to the original entropy as the event horizon radius increased. The rhs of figure 1 shows that the second-order correction term significantly influenced the entropy of a small black hole. In fact, thermal fluctuations have a greater impact on small black holes than on large black holes. Additionally, we demonstrate the effect of spacetime dimensionality on the corrected entropy on the lhs of figure 2. We observed that the corrected entropy changed rapidly and significantly in high-dimensional spacetime. Therefore, it is evident that for small or large black holes, the higher the dimension, the greater is the corrected entropy, whereas this trend does not hold for medium-sized black holes. Furthermore, from the rhs of figure 2, we

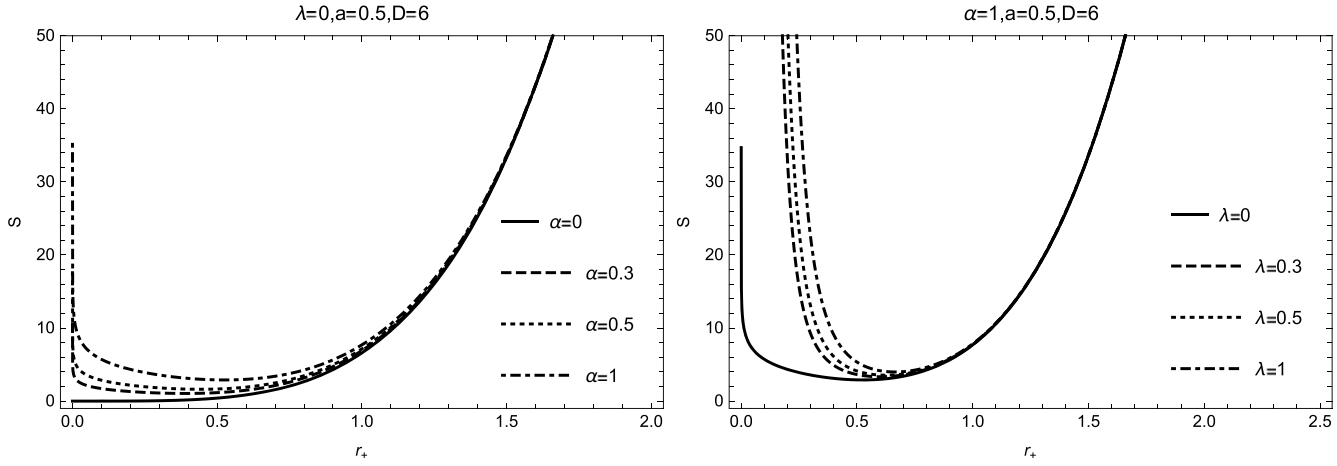

Figure 1. Entropy S in terms of event horizon r_+ for different values of α and λ.

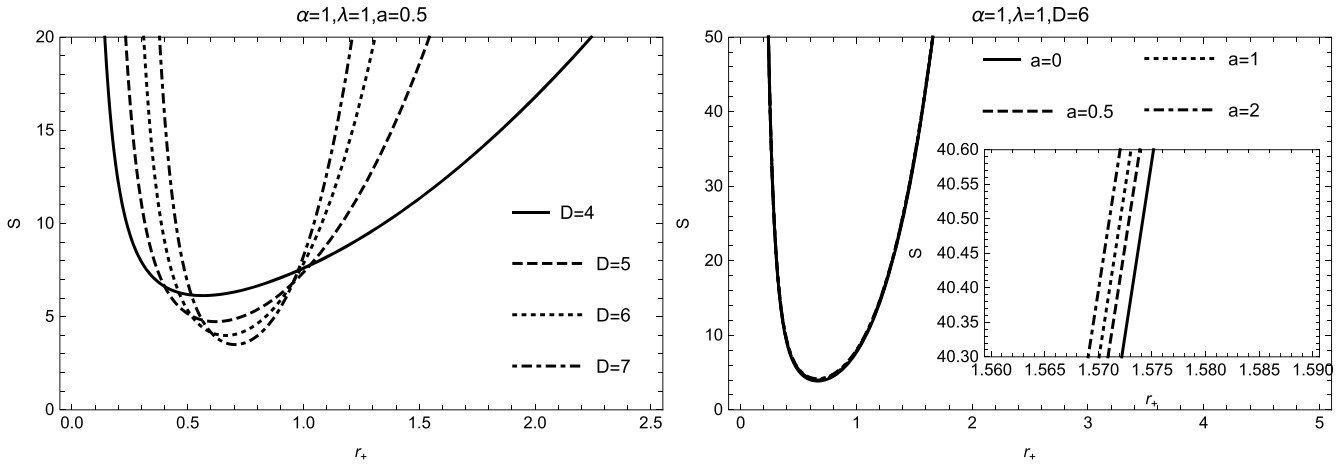

Figure 2. Entropy S in terms of event horizon r_+ for different values of D and a.

deduced that the STVG parameter a led to a slight increase in the corrected entropy.

We can calculate the Helmholtz free energy using the corrected entropy and temperature as

$$F = -\int S\mathrm{d}T = \frac{(D-3)\sqrt{A^2-4GB^2}\,(A-\sqrt{A^2-4GB^2})}{8GB^2\pi} \times\left(\frac{-4r_+^{-D+1}\lambda}{(D-1)\Omega_{D-2}}+\frac{r_+^{D-3}\Omega_{D-2}}{4(D-3)} +\frac{\alpha}{r_+}(D-4 +\ln\left[\frac{(D-3)^2\sqrt{A^2-4GB^2}\,(A-\sqrt{A^2-4GB^2})^2 r_+^{D-4}\Omega_{D-2}}{256G^2B^4\pi^2}\right]\right)\right). \tag{20}$$

To gain a better understanding of the corrected Helmholtz free energy, we depict the Helmholtz free energy as a function of the event horizon for different parameters α, λ, D, and a in figures 3 and 4. In figure 3, we observed that the Helmholtz free energy, without any corrections, is a monotonically increasing function that remains positive. It is noteworthy that the Helmholtz free energy becomes negative for a small black hole under thermal fluctuations but returns to positive as the event horizon radius increases. Conversely, for larger black holes, the presence of the logarithmic correction

term increases the Helmholtz free energy. Furthermore, from the lhs of figure 4, we observed that the influence of spacetime dimensionality on the modified Helmholtz free energy is akin to that of the logarithmic correction. The impact of the STVG parameter a on the corrected Helmholtz free energy is evident on the rhs of figure 4, where it is apparent that the STVG parameter a decreased the corrected Helmholtz free energy.

The internal energy, as one of the thermodynamic quantities, has the thermodynamic relationship $U = F + TS$, i.e.

$$\begin{aligned} U = & \frac{1}{32\pi(D-1)GB^2\Omega_{D-2}} \\ & \times (4GB^2 + A(\sqrt{A^2 - 4GB^2} - A)r_+^{-D-3}) \\ & \times (16(D-3)(D-2)r_+^4\lambda + (D-1)r_+^D\Omega_{D-2} \\ & \times (4(D-4)(D-3)r_+^2\alpha + (D-2)r_+^D\Omega_{D-2})). \end{aligned} \tag{21}$$

Figures 5 and 6 present the behavior of the corrected internal energy with increasing event horizon radius for different parameters α, λ, D, and a. As shown in figure 5, the internal energy has a positive asymptotic value under thermal fluctuations for a small black hole, whereas the effect of thermal fluctuations can be neglected when the event horizon radius is increased. We can see clearly that the higher the dimensionality of the black hole, the larger is the corrected internal energy. However, the corrected internal energy decreases with the increase in the STVG parameter.

Next, we investigated the heat capacity of the black hole, which can be written as $C = (\mathrm{d}U/\mathrm{d}T)_V = \frac{(\mathrm{d}U/\mathrm{d}r)}{(\mathrm{d}T/\mathrm{d}r)}$, where $V = 4\int S_0 \mathrm{d}r_+ = \Omega_{D-2}r_+^{D-1}/(D-1)$ is the black hole volume. Using equations (10) and (21) and the aforementioned definition, one can obtain

$$\begin{aligned} C = & (D-4)\alpha + \frac{4(D-2)r_+^{-D+2}\lambda}{\Omega_{D-2}} \\ & - \frac{1}{4}(D-2)r_+^{D-2}\Omega_{D-2}. \end{aligned} \tag{22}$$

The behavior of the heat capacity is shown in figures 7 and 8. In figure 7, we observed that without any thermal fluctuations, the heat capacity is negative; thus, the black hole is thermodynamically unstable. The existence of thermal fluctuations causes small black holes to have a positive heat capacity; thus, there is a phase transition that shows the transition of the system from unstable to stable. Moreover, the critical point gradually moved to the right when we increased the correction coefficients α and λ. From figure 8, we can see that the phase transition occurs at a larger event horizon radius if the spacetime dimensionality D increases. It is worth mentioning that the heat capacity of a high-dimensional Schwarzschild STVG black hole recovers to that of a Schwarzschild–Tangherlini black hole. In essence, the STVG parameter does not affect the stability conditions of black holes.

4. Weak deflection angle

In this section, we obtain the deflection angle in the weak field limit using the Gauss–Bonnet theorem. For equatorial plane $\theta = \frac{\pi}{2}$ and null geodesic $\mathrm{d}s^2 = 0$, the corresponding optical metric of a high-dimensional Schwarzschild STVG black hole has the following form:

$$\mathrm{d}t^2 = \frac{1}{f^2(r)}\mathrm{d}r^2 + \frac{r^2}{f(r)}\mathrm{d}\varphi^2. \tag{23}$$

Afterward, we can rewrite the optical metric using the coordinate transformation $\mathrm{d}r_* = \frac{1}{f(r)}\mathrm{d}r$ as

$$\mathrm{d}t^2 = \mathrm{d}r_*^2 + \tilde{f}^2(r_*)\mathrm{d}\varphi^2, \tag{24}$$

where $\tilde{f}(r_*) \equiv \sqrt{\frac{r^2}{f(r)}}$.

We obtain the Gaussian optical curvature as follows [72]:

$$\begin{aligned} K = & \frac{\text{Ricci scalar}}{2} = \frac{1}{4}(D-3)r^{1-4D} \\ & \times (4(D-2)G^2q^4r^9 - 2(D-2)mr^{3D} \\ & - 6(D-2)Gq^2r^{6+D} + ((D-1)m^2 \\ & + 4(2D-5)Gq^2)r^{3+2D}). \end{aligned} \tag{25}$$

We can now calculate the deflection angle using the Gauss–Bonnet theorem [78]. The domain $\mathcal{D}$ is deemed to be a subset of a compact, oriented surface, with Gaussian optical curvature K and Euler characteristic number $\chi(\mathcal{D})$, and $\partial\mathcal{D}$ is the piecewise smooth boundary of domain $\mathcal{D}$ with geodesic curvature κ. We consider $\hat{\alpha}_i$ to be the exterior angle at the ith vertex. The Gauss–Bonnet theorem is

$$\int\int_{\mathcal{D}} K\mathrm{d}S + \int_{\partial\mathcal{D}} \kappa\mathrm{d}t + \sum_i \hat{\alpha}_i = 2\pi\chi(\mathcal{D}), \tag{26}$$

where $\mathrm{d}S$ stands for the surface element. In addition, the geodesic curvature κ along a smooth curve γ is written as $\kappa = g(\Delta_{\dot{\gamma}}\dot{\gamma}, \ddot{\gamma})$, where $\ddot{\gamma}$ denotes the unit acceleration vector. We consider that $\mathcal{D}$ is bounded by the geodesics γ_c and γ_R, where γ_R is considered to be perpendicular to γ_c at source S and observer O; thus, $\kappa(\gamma_c) = 0$ by definition. Then, $\sum_i \hat{\alpha}_i = \hat{\alpha}_S + \hat{\alpha}_O$, as well as $\chi(\mathcal{D}) = 1$. Equation (26) reduces to

$$\int\int_{\mathcal{D}} K\mathrm{d}S + \int_{\gamma_R} \kappa(\gamma_R)\mathrm{d}t = \pi. \tag{27}$$

Using the definition of geodesic curvature, the radial part of $\kappa(\gamma_p)$ can be expressed as

$$\kappa(\gamma_p) = (\Delta_{\dot{\gamma}_p}\dot{\gamma}_p)^r = \dot{\gamma}_R^{\phi}(\partial_{\phi}\dot{\gamma}_R^r) + \Gamma^r_{\phi\phi}(\dot{\gamma}_R^{\phi})^2, \tag{28}$$

where $\dot{\gamma}_R$ represents the tangent vector of geodesics γ_R, and $\Gamma^r_{\phi\phi}$ is a Christoffel symbol. When we consider $\gamma_R := R = \text{const}$, the first term on the right side of the

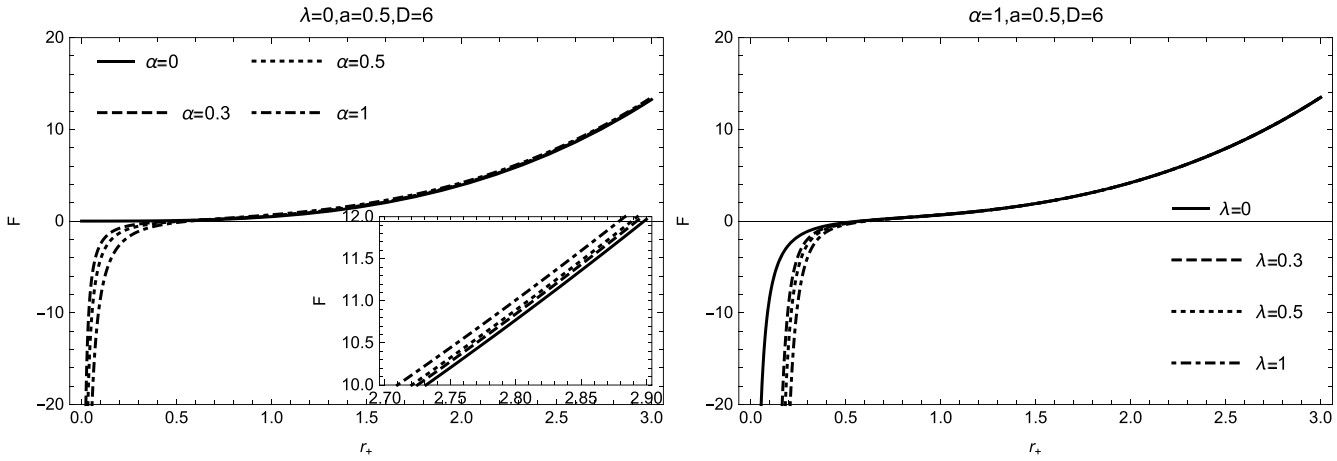

Figure 3. Helmholtz free energy F in terms of event horizon r_+ for different values of α and λ.

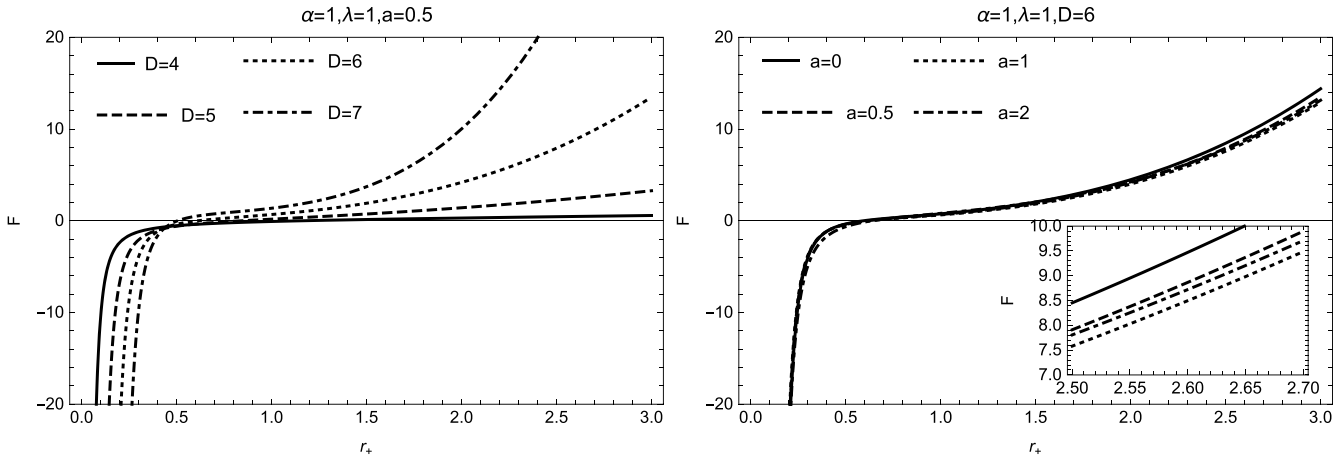

Figure 4. Helmholtz free energy F in terms of event horizon r_+ for different values of D and a.

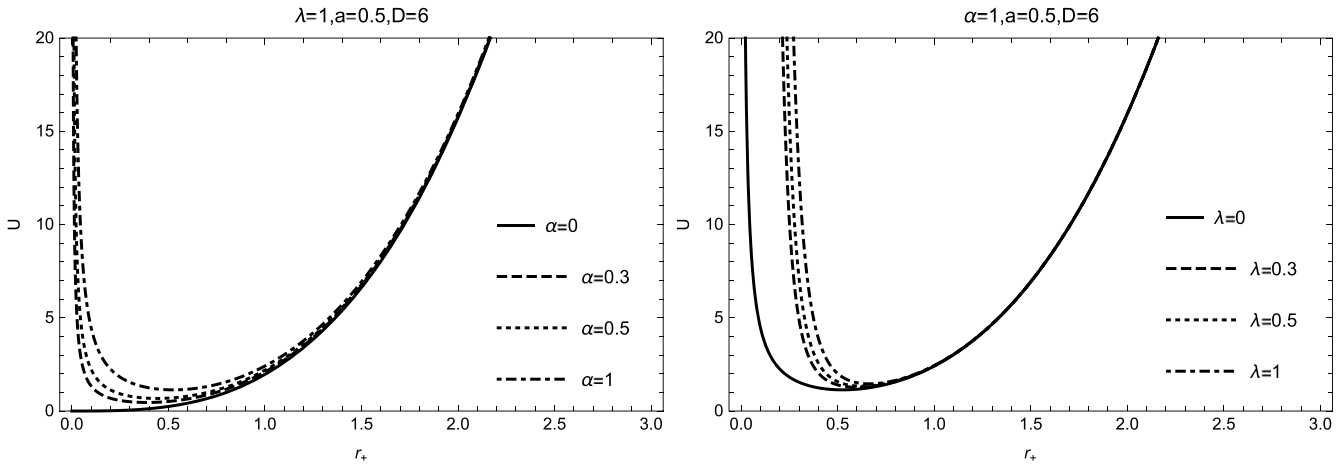

Figure 5. Internal energy U in terms of event horizon r_+ for different values of α and λ.

preceding equation equals zero, and the second term is $\frac{1}{R}$; thus, $\kappa(\gamma_R)$ reduces to $\frac{1}{R}$. We can make a change in variables $\mathrm{d}t$ using the relevant optical metric (24), which can be rewritten as $\mathrm{d}t = R\mathrm{d}\varphi$. Equation (27) becomes

$$\iint_{\mathcal{D}} K\mathrm{d}S + \int_0^{\pi+\hat{\alpha}_b} \mathrm{d}\varphi = \pi. \tag{29}$$

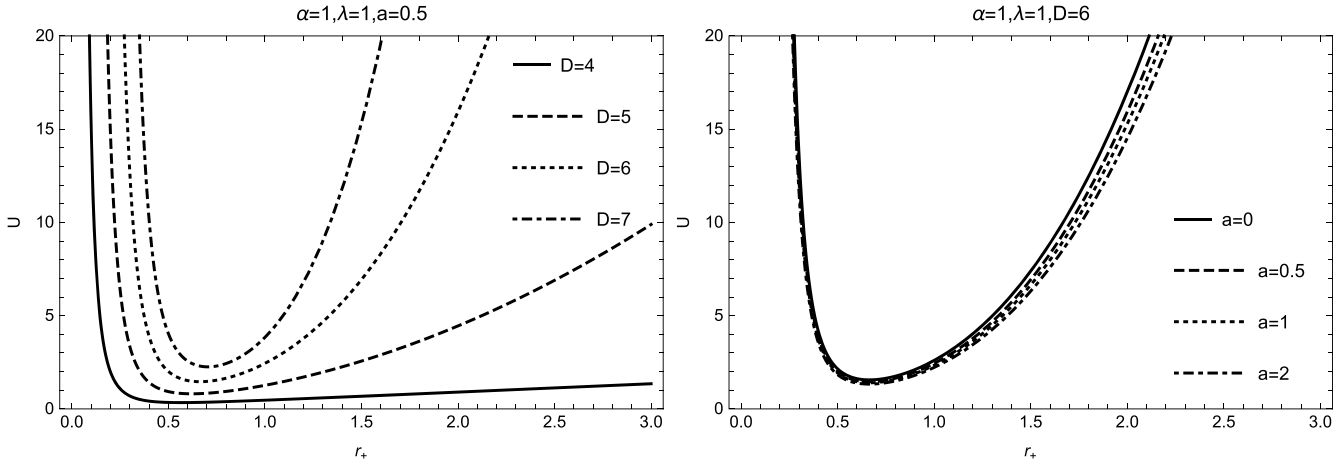

Figure 6. Internal energy U in terms of event horizon r_+ for different values of D and a.

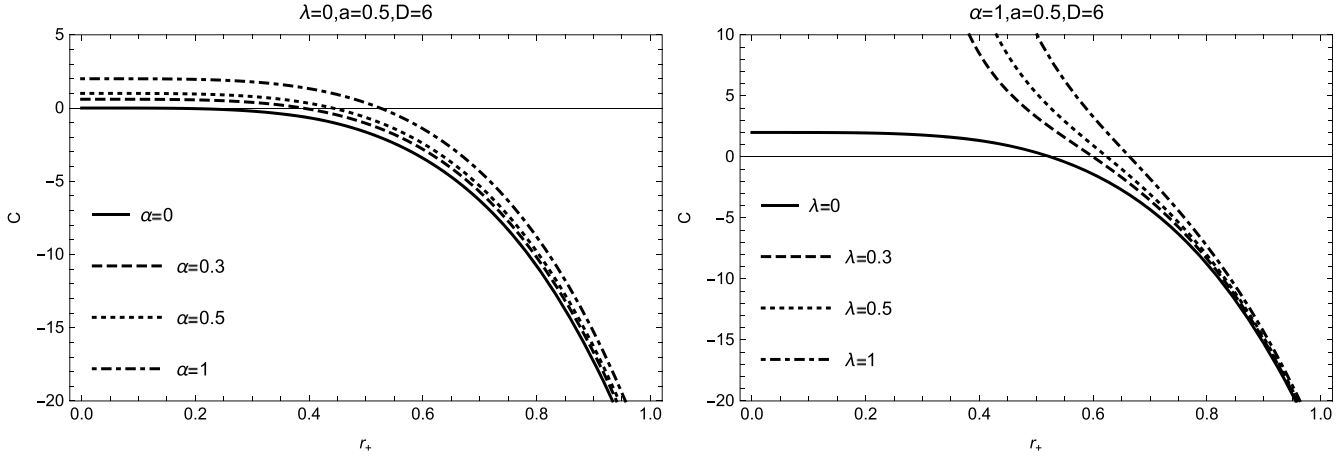

Figure 7. Heat capacity C in terms of event horizon r_+ for different values of α and λ.

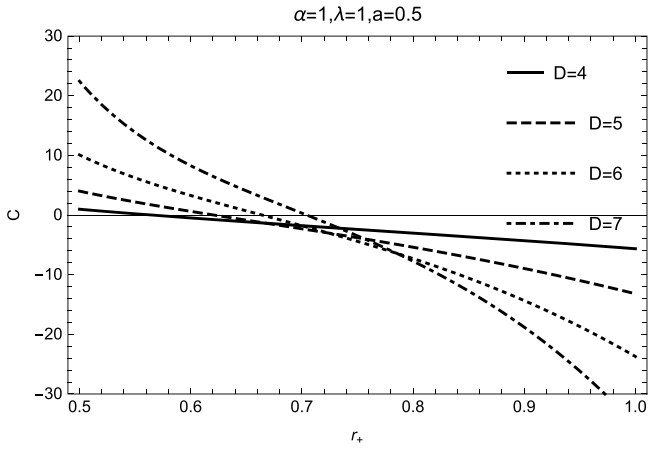

Figure 8. Heat capacity C in terms of event horizon r_+ for different values of D.

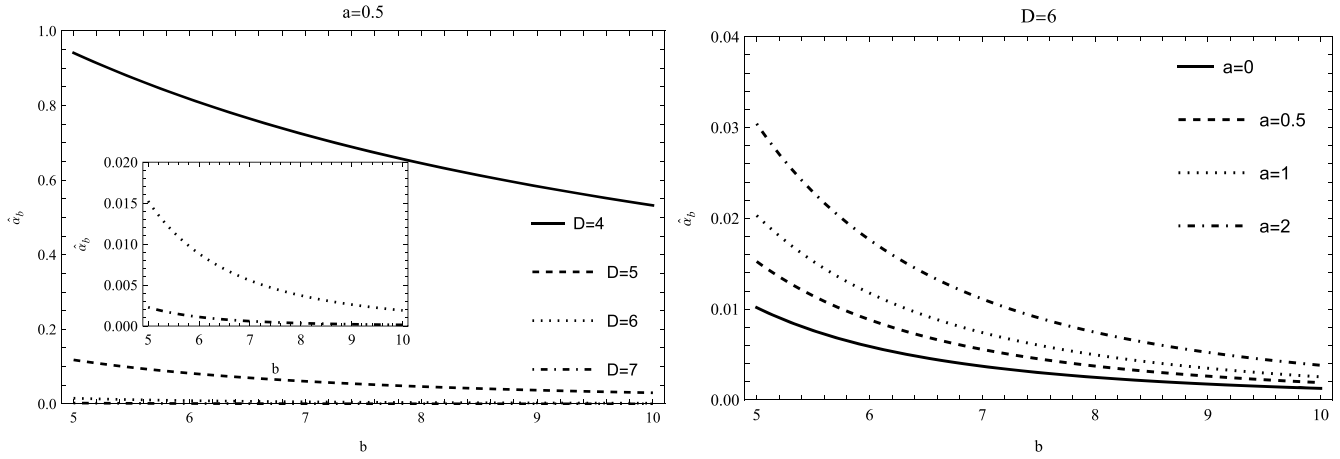

Figure 9. Deflection angle $\hat{\alpha}_b$ in terms of impact parameter b for different values of D and a. The black hole mass is $M = 1$.

Finally, we obtain the deflection angle [78]

$$\hat{\alpha}_b = -\int_0^{\pi}\int_{b/\sin\phi}^{\infty} K\mathrm{d}S. \tag{30}$$

We can now calculate the deflection angle of a high-dimensional Schwarzschild black hole in the STVG theory for different spacetime dimensionalities. As an example, we calculated the deflection angle when $D = 4$, 5, 6, and 7:

$$\begin{aligned}
\hat{\alpha}_{D=4} &= \frac{2m}{b} - \frac{3m^2\pi}{16b^2} - \frac{3G\pi q^2}{4b^2} \\
&\quad + \frac{4Gmq^2}{3b^3} + O\left(\frac{q^4}{b^4}\right), \\
\hat{\alpha}_{D=5} &= \frac{3m\pi}{4b^2} - \frac{3m^2\pi}{16b^4} - \frac{15G\pi q^2}{16b^4} \\
&\quad + \frac{15Gm\pi q^2}{32b^6} + O\left(\frac{q^4}{b^8}\right), \\
\hat{\alpha}_{D=6} &= \frac{8m}{3b^3} - \frac{25m^2\pi}{128b^6} - \frac{35G\pi q^2}{32b^6} \\
&\quad + \frac{512Gmq^2}{315b^9} + O\left(\frac{q^4}{b^{12}}\right), \\
\hat{\alpha}_{D=7} &= \frac{15\pi m}{16b^4} - \frac{105m^2\pi}{512b^8} - \frac{315G\pi q^2}{256b^8} \\
&\quad + \frac{1155Gm\pi q^2}{2048b^{12}} + O\left(\frac{q^4}{b^{16}}\right).
\end{aligned} \tag{31}$$

The behavior of the deflection angle with respect to the impact parameter for different values of D and a is shown in figure 9. It is clear that the higher the black hole dimension, the smaller is the deflection angle. However, the STVG parameter has an increasing effect on the deflection angle, i.e. a high-dimensional Schwarzschild STVG black hole leads to a larger deflection angle than a Schwarzschild–Tangherlini black hole.

5. Greybody factor

In this section, we study the bounds on greybody factor for the massless scalar field. The massless scalar field Φ is represented by the Klein–Gordon equation [98],

$$\frac{1}{\sqrt{-g}}\partial_\mu(\sqrt{-g}\,g^{\mu\nu}\partial_\nu)\Phi = 0, \tag{32}$$

where g is the determinant of the metric tensor. To separate the radial and angular variables, we have an ansatz $\Phi = \mathrm{e}^{-\mathrm{i}\omega t}Y_{\boldsymbol{lm}}(\theta,\varphi)\Psi(r)/r^{\frac{D-2}{2}}$ and make a change $\mathrm{d}r_* = \frac{\mathrm{d}r}{f(r)}$. Substituting the aforementioned definitions and metric function equation (4) into equation (32), we obtained a Schrödinger-like wave expression:

$$\frac{\mathrm{d}^2\Psi(r)}{\mathrm{d}^2 r_*} + [\omega^2 - V_{\mathit{eff}}(r)]\Psi(r) = 0, \tag{33}$$

in which ω denotes frequency, and l and $\boldsymbol{m}$ are the azimuthal quantum number and spherical harmonic index, respectively.

The effective potential $V_{\mathrm{eff}}(r)$ can be written as

$$\begin{aligned}
V_{\mathrm{eff}}(r) = f(r)\Bigg[&\frac{l(D+l-3)}{r^2} + \frac{(D-2)(D-4)f(r)}{4r^2} \\
&+ \frac{(D-2)f'(r)}{2r}\Bigg].
\end{aligned} \tag{34}$$

To better understand the effect of the dimensionality of the spacetime and STVG parameter on the effective potential, we visualized the effective potential with respect to the black hole radius for different values of D and a, as shown in figure 10. Obviously, the dimensionality of spacetime caused an increase in the effective potential, whereas the STVG parameter has the opposite effect. We can expect the behavior of the greybody factor from the effective potential.

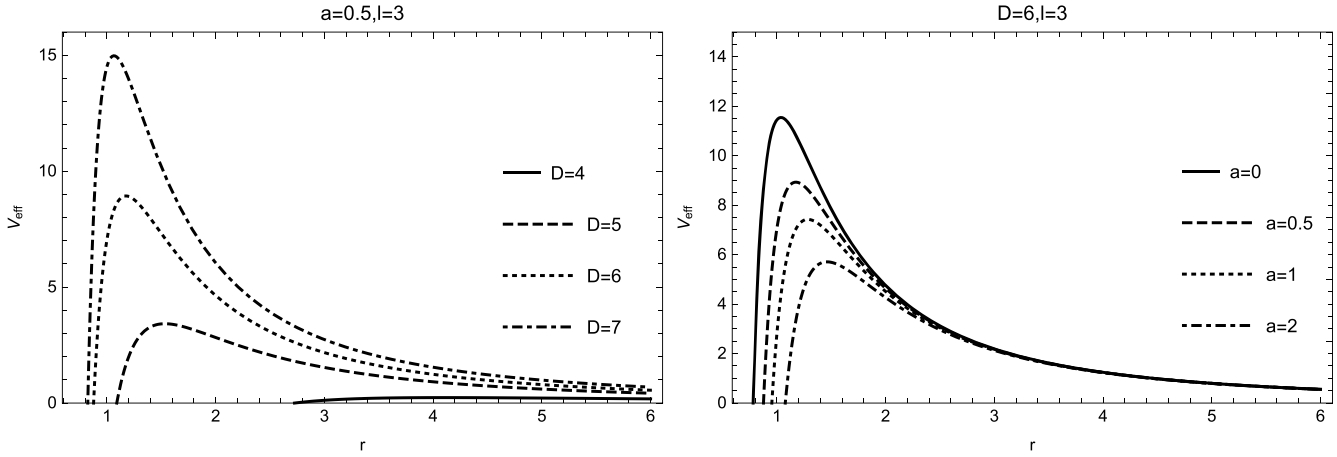

Figure 10. Behavior of effective potential V_{eff} for different values of D and a. The black hole mass is $M = 1$.

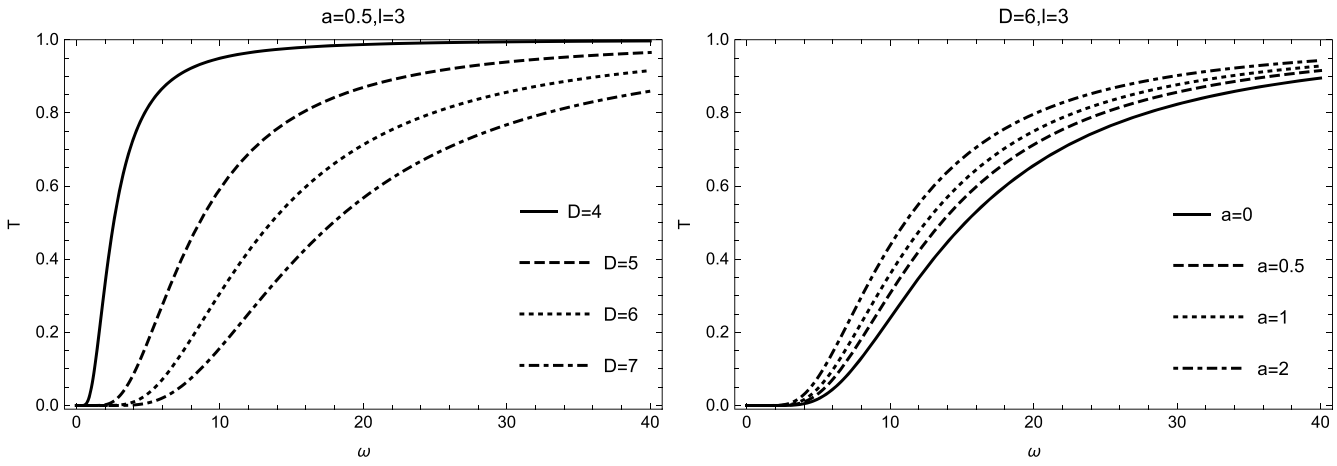

Figure 11. Greybody factor $T(\omega)$ in terms of frequency ω for different values of D and a. The black hole mass is $M = 1$.

The bounds on the greybody factor can be expressed as [40]

$$T(\omega) \geqslant \operatorname{sech}^2\left[\int_{-\infty}^{\infty} \frac{\sqrt{(h')^2 + (\omega^2 - V_{\text{eff}} - h^2)^2}}{2h} \mathrm{d}r_*\right], \tag{35}$$

where $h \equiv h(r_*)$ and $h(r_*) > 0$; h is an arbitrary function and satisfies $h(-\infty) = h(\infty) = \omega$, and there were two particular functional forms of h considered in [40]. In this study, we considered only the case $h = \omega$. Thus, equation (35) was rewritten as

$$T(\omega) \geqslant \operatorname{sech}^2\left[\frac{1}{2\omega}\int_{r_+}^{\infty} \frac{V_{\text{eff}}}{f(r)} \mathrm{d}r\right]. \tag{36}$$

After expanding the integral, we obtained the lower bounds on the greybody factor

$$T(\omega) \geqslant \operatorname{sech}^2\left[\frac{1}{2\omega}\left(\frac{1}{4r_+}(8 - 6D + D^2 - 12l + 4lD + 4l^2) - \frac{(D-2)(3D-8)Gq^2}{4(2D-5)} r_+^{5-2D} + \frac{(D-2)m}{4} r_+^{2-D}\right)\right]. \tag{37}$$

Figure 11 demonstrates the behavior of the greybody factor for the high-dimensional Schwarzschild black hole in the STVG theory. From the left panel, we observed that the greybody factor decreased with an increase in the dimension. In other words, the greybody factor is suppressed in high-dimensional spacetime. This indicates that fewer massless scalar particles pass through the potential barrier and reach spatial infinity in a higher-dimensional black hole. Additionally, we observed that as the STVG parameter a increased, the greybody factor increased. That is, more radiation passes through the potential barrier and reaches infinity as the STVG parameter increases.

6. Conclusions

In this study, we analyzed the thermal fluctuations, weak deflection angle, and greybody factor of a high-dimensional Schwarzschild STVG black hole.

First, we evaluated the influence of the logarithmic and higher-order corrections of entropy on the Helmholtz free energy, internal energy, and heat capacity. We compared the corrected and uncorrected thermodynamic properties. Overall, the corrected entropy as a consequence of thermal fluctuations

first decreased and then increased, and the impact of thermal fluctuations was significant for a small black hole. Because of the effect of the dimensionality of spacetime, the curves of the corrected entropy have different intersections. This means that for a small or large black hole, the corrected entropy increases as the spacetime dimensionality increases, whereas the middle black hole is not the case. The presence of the STVG parameter led to a slight increase in the corrected entropy. The black hole with small values of the event horizon radius possessed negative Helmholtz free energy because of thermal fluctuations. The Helmholtz free energy increased monotonically with increasing values of the parameters D and a for a small black hole. For a larger black hole, the parameters D and a have opposite effects on the Helmholtz free energy. The internal energy remained positive, and its behavior was similar to that of the corrected entropy. The internal energy increased with an increase in the dimensions, whereas it decreased as the STVG parameter increased. In addition, we have found that thermal fluctuations make the small black hole more stable from the analysis of Helmholtz free energy and heat capacity in all dimensional cases, and the heat capacity is independent of the STVG parameter.

Second, we calculated the weak deflection angle using the Gauss–Bonnet theorem and presented expressions for $D = 4$, 5, 6, and 7. We pointed out that in higher-dimensional spacetime, the weak deflection angle became weaker, but the presence of the STVG parameter resulted in an increase in the deflection angle. In the future, we can calculate the mass of the black hole more accurately by measuring the weak deflection angle of light caused by a black hole. This is important for studying the dynamics and evolution of black holes. It is worth emphasizing that the STVG theory does not include dark matter, but it can account for the rotation curves of galaxies, which require the presence of dark matter to explain the phenomena in the general relativity theory. Therefore, by comparing the predictions of such theories regarding weak deflection angles with actual observational data, clues may be provided regarding which theories are more effective in describing our universe.

Finally, we computed the greybody factor of the massless scalar field and then analyzed the effect of the spacetime dimensionality and STVG parameter on the greybody factor. We discovered that the four-dimensional black hole had the largest greybody factor values, whereas the seven-dimensional black hole had the smallest values. Moreover, when the STVG parameter increased, the greybody factor increased. We found that more radiation can reach spatial infinity in a four-dimensional black hole with a larger value of STVG parameter.

Acknowledgments

This work was supported by the National Natural Science Foundation of China (Grant No. 12065012), Yunnan Fundamental Research Projects (202301AS070029), and Yunnan High-Level Talent Training Support Plan Young & Elite Talents Project (Grant No. YNWR-QNBJ-2018-360).

References

[1] Astier P and Pain R 2012 Observational evidence of the accelerated expansion of the universe *C. R. Physique* **13** 521–38
[2] Moffat J W and Rahvar S 2013 The MOG weak field approximation and observational test of galaxy rotation curves *Mon. Not. R. Astron. Soc.* **436** 1439–51
[3] Ade P A R *et al* 2016 Planck 2015 results. XIII. Cosmological parameters *Astron. Astrophys.* **594** A13
[4] Moffat J W 2015 Black Holes in modified gravity (MOG) *Eur. Phys. J.* C **75** 175
[5] Moffat J W 2006 Scalar-tensor-vector gravity theory *J. Cosmol. Astropart. Phys.* JCAP03(2006)004
[6] Brownstein J R and Moffat J W 2006 Galaxy rotation curves without non-baryonic dark matter *Astrophys. J.* **636** 721–41
[7] Roshan M 2015 Exact cosmological solutions for MOG *Eur. Phys. J.* C **75** 405
[8] Moffat J W 2021 Regular rotating MOG dark compact object *Eur. Phys. J.* C **81** 119
[9] Pérez D and Romero G E 2019 Exact cosmological black hole solutions in scalar tensor vector gravity *Class. Quantum Grav.* **36** 245022
[10] Davari Z and Rahvar S 2021 MOG cosmology without dark matter and the cosmological constant *Mon. Not. R. Astron. Soc.* **507** 3387–99
[11] Jamali S, Roshan M and Amendola L 2018 On the cosmology of scalar-tensor-vector gravity theory *J. Cosmol. Astropart. Phys.* JCAP01(2018)048
[12] Nozari K, Saghafi S and Aliyan F 2023 Accretion onto a static spherically symmetric regular MOG dark compact object *Eur. Phys. J.* C **83** 449
[13] Saghafi S and Nozari K 2023 Hawking-Like radiation as tunneling from a cosmological black hole in modified gravity: semiclassical approximation and beyond *Gen. Relativ. Gravit.* **55** 20
[14] Al-Badawi A 2023 Probing regular MOG static spherically symmetric spacetime using greybody factors and quasinormal modes *Eur. Phys. J.* C **83** 620
[15] Al-Badawi A and Jawad A 2024 Study of quasinormal modes, greybody factors, and thermodynamics within a regular MOG black hole surrounded by quintessence *Eur. Phys. J.* C **84** 115
[16] Bekenstein J D 1973 Black holes and entropy *Phys. Rev.* D **7** 2333–46
[17] Strominger A and Vafa C 1996 Microscopic origin of the Bekenstein-Hawking entropy *Phys. Lett.* B **379** 99–104
[18] Aharony O, Gubser S S, Maldacena J M, Ooguri H and Oz Y 2000 Large N field theories, string theory and gravity *Phys. Rep.* **323** 183–386
[19] Emparan R and Reall H S 2008 Black holes in higher dimensions *Living Rev. Relativ.* **11** 6
[20] Tangherlini F R 1963 Schwarzschild field in n dimensions and the dimensionality of space problem *Nuovo Cimento* **27** 636–51
[21] Myers R C and Perry M J 1986 Black holes in higher dimensional space-times *Ann. Phys., NY* **172** 304
[22] Cai X C and Miao Y G 2021 High-dimensional Schwarzschild black holes in scalar–tensor–vector gravity theory *Eur. Phys. J.* C **81** 559
[23] Hawking S W 1974 Black hole explosions *Nature* **248** 30–1
[24] Hawking S W 1975 Particle creation by black holes *Commun. Math. Phys.* **43** 199–220
[25] Easther R and Lowe D A 1999 Holography, cosmology, and the second law of thermodynamics *Phys. Rev. Lett.* **82** 4967–70
[26] Mandal S, Das S, Gogoi D J and Pramanik A 2023 Leading-order corrections to the thermodynamics of Rindler modified Schwarzschild black hole *Phys. Dark Universe* **42** 101349

[27] Pourhassan B, Kokabi K and Rangyan S 2017 Thermodynamics of higher dimensional black holes with higher order thermal fluctuations *Gen. Relativ. Gravit.* **49** 144

[28] Chen X, Huang X, Chen J and Wang Y 2021 Effect of thermal fluctuation on the thermodynamics of GMGHS black hole *Gen. Relativ. Gravit.* **53** 9

[29] Das S, Majumdar P and Bhaduri R K 2002 General logarithmic corrections to black hole entropy *Class. Quantum Grav.* **19** 2355–68

[30] Upadhyay S 2017 Quantum corrections to thermodynamics of quasitopological black holes *Phys. Lett.* B **775** 130–9

[31] Dehghani M 2018 Thermodynamics of charged dilatonic BTZ black holes in rainbow gravity *Phys. Lett.* B **777** 351–60

[32] Jawad A and Shahzad M U 2017 Effects of thermal fluctuations on non-minimal regular magnetic black hole *Eur. Phys. J.* C **77** 349

[33] Shahzad M U and Jawad A 2019 Thermodynamics of black holes with higher order corrected entropy *Can. J. Phys.* **97** 742–51

[34] Sharif M and Akhtar Z 2021 Study of thermal fluctuations in five-dimensional rotating regular black hole *Chin. J. Phys.* **71** 669–82

[35] Khan Y H and Ganai P A 2022 Remnants and thermal corrections in Horndeski black holes with non-minimal kinetic coupling *Eur. Phys. J. Plus* **137** 827

[36] Ama-Tul-Mughani Q, Waseem A, Salam W U and Jawad A 2022 Greybody factor and thermal fluctuations of rotating regular black hole bounded by PFDM *Chin. J. Phys.* **77** 2213–27

[37] Upadhyay S, Nadeem-ul-islam and Ganai P A 2022 A modified thermodynamics of rotating and charged BTZ black hole *J. Hologr. Appl. Phys.* **2** 25–48

[38] Khan Y H, Upadhyay S and Ganai P A 2021 Stability of remnants of Bardeen regular black holes in presence of thermal fluctuations *Mod. Phys. Lett.* A **36** 2130023

[39] Barman S 2020 The Hawking effect and the bounds on greybody factor for higher dimensional Schwarzschild black holes *Eur. Phys. J.* C **80** 50

[40] Konoplya R A 2020 Quantum corrected black holes: quasinormal modes, scattering, shadows *Phys. Lett.* B **804** 135363

[41] Boonserm P and Visser M 2008 Bounding the greybody factors for Schwarzschild black holes *Phys. Rev.* D **78** 101502

[42] Boonserm P, Chatrabhuti A, Ngampitipan T and Visser M 2014 Greybody factors for Myers–Perry black holes *J. Math. Phys.* **55** 112502

[43] Boonserm P, Ngampitipan T and Wongjun P 2018 Greybody factor for black holes in dRGT massive gravity *Eur. Phys. J.* C **78** 492

[44] Okyay M and Övgün A 2022 Nonlinear electrodynamics effects on the black hole shadow, deflection angle, quasinormal modes and greybody factors *J. Cosmol. Astropart. Phys.* JCAP01(2022)009

[45] Konoplya R A 2003 Quasinormal behavior of the d-dimensional Schwarzschild black hole and higher order WKB approach *Phys. Rev.* D **68** 024018

[46] Kokkotas K D, Konoplya R A and Zhidenko A 2011 Quasinormal modes, scattering and Hawking radiation of Kerr-Newman black holes in a magnetic field *Phys. Rev.* D **83** 024031

[47] Konoplya R A, Zinhailo A F and Stuchlik Z 2020 Quasinormal modes and Hawking radiation of black holes in cubic gravity *Phys. Rev.* D **102** 044023

[48] Li Q, Ma C, Zhang Y, Lin Z W and Duan P F 2022 Gray-body factor and absorption of the Dirac field in ESTGB gravity *Chin. J. Phys.* **77** 1269–77

[49] Konoplya R A and Zhidenko A 2023 Analytic expressions for quasinormal modes and grey-body factors in the eikonal limit and beyond *Class. Quantum Grav.* **40** 245005

[50] Harris C M and Kanti P 2003 Hawking radiation from a (4+n)-dimensional black hole: exact results for the Schwarzschild phase *J. High Energy Phys.* JHEP10(2003)014

[51] Catalán M, Cisternas E, González P A and Vásquez Y 2016 Quasinormal modes and greybody factors of a four-dimensional Lifshitz black hole with z = 0 *Astrophys. Space Sci.* **361** 189

[52] Abedi J and Arfaei H 2014 Fermionic greybody factors in dilaton black holes *Class. Quantum Grav.* **31** 195005

[53] Lewis A and Challinor A 2006 Weak gravitational lensing of the CMB *Phys. Rep.* **429** 1–65

[54] Peloton J, Schmittfull M, Lewis A, Carron J and Zahn O 2017 Full covariance of CMB and lensing reconstruction power spectra *Phys. Rev.* D **95** 043508

[55] Pratten G and Lewis A 2016 Impact of post-Born lensing on the CMB *J. Cosmol. Astropart. Phys.* JCAP08(2016)047

[56] Tsukamoto N, Kitamura T, Nakajima K and Asada H 2014 Gravitational lensing in Tangherlini spacetime in the weak gravitational field and the strong gravitational field *Phys. Rev.* D **90** 064043

[57] Chen S and Jing J 2015 Strong gravitational lensing for the photons coupled to Weyl tensor in a Schwarzschild black hole spacetime *J. Cosmol. Astropart. Phys.* JCAP10(2015)002

[58] Chen S, Wang S, Huang Y, Jing J and Wang S 2017 Strong gravitational lensing for the photons coupled to a Weyl tensor in a Kerr black hole spacetime *Phys. Rev.* D **95** 104017

[59] Wang S, Chen S and Jing J 2016 Strong gravitational lensing by a Konoplya-Zhidenko rotating non-Kerr compact object *J. Cosmol. Astropart. Phys.* JCAP11(2016)020

[60] Lu X, Yang F W and Xie Y 2016 Strong gravitational field time delay for photons coupled to Weyl tensor in a Schwarzschild black hole *Eur. Phys. J.* C **76** 357

[61] Zhao S S and Xie Y 2016 Strong field gravitational lensing by a charged Galileon black hole *J. Cosmol. Astropart. Phys.* JCAP07(2016)007

[62] Zhao S S and Xie Y 2017 Strong deflection gravitational lensing by a modified Hayward black hole *Eur. Phys. J.* C **77** 272

[63] Zhang R, Jing J and Chen S 2017 Strong gravitational lensing for black holes with scalar charge in massive gravity *Phys. Rev.* D **95** 064054

[64] Abbas G, Mahmood A and Zubair M 2020 Strong gravitational lensing for photon coupled to weyl tensor in Kiselev black hole *Chin. Phys.* C **44** 095105

[65] Bergliaffa S E P, Filho E E D and Maier R 2020 Strong lensing and nonminimally coupled electromagnetism *Phys. Rev.* D **101** 124038

[66] Wang C Y, Shen Y F and Xie Y 2019 Weak and strong deflection gravitational lensings by a charged Horndeski black hole *J. Cosmol. Astropart. Phys.* JCAP04(2019)022

[67] Kumaran Y and Övgün A 2020 Weak deflection angle of extended uncertainty principle black holes *Chin. Phys.* C **44** 025101

[68] Javed W, Khadim M B and Övgün A 2020 Weak gravitational lensing by Bocharova–Bronnikov–Melnikov–Bekenstein black holes using Gauss–Bonnet theorem *Eur. Phys. J. Plus* **135** 595

[69] Javed W, Abbas J, Kumaran Y and Övgün A 2021 Weak deflection angle by asymptotically flat black holes in Horndeski theory using Gauss-Bonnet theorem *Int. J. Geom. Methods Mod. Phys.* **18** 2150003

[70] Xu X, Jiang T and Jia J 2021 Deflection angle with electromagnetic interaction and gravitational-electromagnetic dual lensing *J. Cosmol. Astropart. Phys.* JCAP08(2021)022

[71] Javed W, Hamza A and Övgün A 2021 Weak deflection angle and shadow by tidal charged black hole *Universe* **7** 385
[72] Gao Y X and Xie Y 2021 Gravitational lensing by hairy black holes in Einstein-scalar-Gauss-Bonnet theories *Phys. Rev.* D **103** 043008
[73] Javed W, Hamza A and Övgün A 2020 Effect of nonlinear electrodynamics on the weak field deflection angle by a black hole *Phys. Rev.* D **101** 103521
[74] Tsukamoto N 2021 Gravitational lensing by a photon sphere in a Reissner-Nordström naked singularity spacetime in strong deflection limits *Phys. Rev.* D **104** 124016
[75] Tsukamoto N 2022 Gravitational lensing by a Bronnikov-Kim wormhole under a weak-field approximation and in a strong deflection limit *Phys. Rev.* D **105** 064013
[76] Kumar R, Islam S U and Ghosh S G 2020 Gravitational lensing by charged black hole in regularized 4*D* Einstein–Gauss–Bonnet gravity *Eur. Phys. J.* C **80** 1128
[77] Moumni H, El, Masmar K and Övgün A 2022 Weak deflection angle of light in two classes of black holes in nonlinear electrodynamics via Gauss–Bonnet theorem *Int. J. Geom. Methods Mod. Phys.* **19** 2250094
[78] Gibbons G W and Werner M C 2008 Applications of the Gauss-Bonnet theorem to gravitational lensing *Class. Quantum Grav.* **25** 235009
[79] Ishihara A, Suzuki Y, Ono T, Kitamura T and Asada H 2016 Gravitational bending angle of light for finite distance and the Gauss-Bonnet theorem *Phys. Rev.* D **94** 084015
[80] Islam S U, Kumar R and Ghosh S G 2020 Gravitational lensing by black holes in the 4*D* Einstein-Gauss-Bonnet gravity *J. Cosmol. Astropart. Phys.* JCAP09(2020)030
[81] Zhu T, Wu Q, Jamil M and Jusufi K 2019 Shadows and deflection angle of charged and slowly rotating black holes in Einstein-Æther theory *Phys. Rev.* D **100** 044055
[82] Sakallı I and Övgün A 2017 Hawking radiation and deflection of light from Rindler modified Schwarzschild black hole *Europhys. Lett.* **118** 60006
[83] Jusufi K, Övgün A, Saavedra J, Vásquez Y and González P A 2018 Deflection of light by rotating regular black holes using the Gauss-Bonnet theorem *Phys. Rev.* D **97** 124024
[84] Övgün A, Sakallı I and Saavedra J 2019 Weak gravitational lensing by Kerr-MOG black hole and Gauss–Bonnet theorem *Ann. Phys., NY* **411** 167978
[85] Li Z, Zhang G and Övgün A 2020 Circular orbit of a particle and weak gravitational lensing *Phys. Rev.* D **101** 124058
[86] Javed W, Khadim M B, Övgün A and Abbas J 2020 Weak gravitational lensing by stringy black holes *Eur. Phys. J. Plus* **135** 314
[87] Belhaj A, Benali M, El Balali A, El Moumni H and E Ennadifi S 2020 Deflection angle and shadow behaviors of quintessential black holes in arbitrary dimensions *Class. Quantum Grav.* **37** 215004
[88] Nozari K and Saghafi S 2023 Asymptotically locally flat and AdS higher-dimensional black holes of Einstein–Horndeski–Maxwell gravity in the light of EHT observations: shadow behavior and deflection angle *Eur. Phys. J.* C **83** 588
[89] Crispino L C B, Dolan S R and Oliveira E S 2009 Scattering of massless scalar waves by Reissner-Nordström black holes *Phys. Rev.* D **79** 064022
[90] Mureika J R, Moffat J W and Faizal M 2016 Black hole thermodynamics in MOdified Gravity (MOG) *Phys. Lett.* B **757** 528–36
[91] More S S 2005 Higher order corrections to black hole entropy *Class. Quantum Grav.* **22** 4129–40
[92] Pourhassan B and Faizal M 2016 Thermodynamics of a sufficient small singly spinning Kerr-AdS black hole *Nucl. Phys.* B **913** 834–51
[93] Pourhassan B, Farahani H and Upadhyay S 2019 Thermodynamics of higher-order entropy corrected Schwarzschild–Beltrami–de Sitter black hole *Int. J. Mod. Phys.* **A34** 1950158
[94] Pourhassan B, Faizal M and Ketabi S A 2018 Logarithmic correction of the BTZ black hole and adaptive model of Graphene *Int. J. Mod. Phys.* D **27** 1850118
[95] Bubuianu L and Vacaru S I 2019 Black holes with MDRs and Bekenstein–Hawking and Perelman entropies for Finsler–Lagrange–Hamilton Spaces *Ann. Phys., NY* **404** 10–38
[96] Sharif M and Khan A 2022 Thermal fluctuations, quasi-normal modes and phase transitions of regular black hole *Chin. J. Phys.* **77** 1885–902
[97] Sharif M and Ama-Tul-Mughani Q 2020 Phase transition and thermal fluctuations of quintessential Kerr–Newman-AdS black hole *Phys. Dark Universe* **30** 100723
[98] Berti E, Cardoso V and Starinets A O 2009 Quasinormal modes of black holes and black branes *Class. Quantum Grav.* **26** 163001